Key Points:
- Offset between lithospheric and crustal scale inherited shear zones controls their reactivation upon extension
- Crustal scale shear zones far from lithospheric scale shear zones (suture) are left unreactivated and preserve orogenic structure
- Wide margin development reactivates inherited contractional structures, while narrow margin reactivates inherited extensional structures

Correspondence to:
C. A. Salazar-Mora,
claudio.mora@usp.br

The Wilson Cycle and Effects of Tectonic Structural Inheritance on Rifted Passive Margin Formation

Claudio A. Salazar-Mora[1,2] , Ritske S. Huismans[1] , Haakon Fossen[1,3] , and Marcos Egydio-Silva[2]

[1]Department of Earth Sciences, University of Bergen, Bergen, Norway, [2]Geosciences Institute, São Paulo University, São Paulo, Brazil, [3]University Museum of Bergen – The Natural History Collections, University of Bergen, Bergen, Norway

Abstract The parallelism between older collisional belts and younger rift systems is widely known and particularly well portrayed along the Atlantic Ocean. How tectonic inherited and new-formed shear zones control rift nucleation and the final architecture of rifted conjugate passive margins is still poorly understood. Here we present lithospheric-scale thermo-mechanical numerical models that self-consistently create extensional and contractional tectonic inheritance, where prior extension and contraction are systematically varied. Our results show that (1) initial reactivation occurs along the former lithospheric suture zones; (2) upper crustal thick-skinned basement thrusts are partially or fully reactivated depending on the amount of prior contraction and size of the orogen; (3) with a small amount of contraction, thick-skinned thrusts are efficiently reactivated in extension and provide the template for rifted margin formation; (4) with larger amounts of contraction, thick-skinned thrusts distal to the lithospheric suture zone do not reactivate in extension; and (5) reactivation of prior contractional shear zones dominates during the early stages of rifting, while during the final stage of margin formation new-formed extensional shear zones dominate. Force balance analysis predicts an inverse relation between midcrustal viscosity and the maximum offset for reactivation of weak upper crustal structures. Force balance also predicts that the degree of weakening or healing of the weak suture and the thermal thinning of the necking area control at which stage suture reactivation is deactivated and extension proceeds by mantle lithosphere thermal necking. Two rifted conjugate margins with orogenic inheritance in the North and South Atlantic are used for comparison.

1. Introduction

During the Wilson cycle, continental lithosphere is repeatedly weakened and reworked at its margins (Wilson, 1966) during subduction, orogeny, and rifting, while continental nuclei remain undeformed. Preexisting shear zones within the lithosphere have been suggested to be a key factor controlling rift development (e.g., Petersen & Schiffer, 2016; Schiffer et al., 2015), as illustrated by the parallelism between older orogenic belts and younger rift systems during the breakup of Western Gondwana and the development of the North, Central, and South Atlantic rifted margins (Buiter & Torsvik, 2014; Piquè & Laville, 1996; Vauchez et al., 1997). Cratonic lithosphere is strong and tectonically stable owing to dehydration, a prevalence of refractory crustal composition (Peslier et al., 2010) and low heat flux conditions (Sleep, 2003). On the other hand, younger continental lithosphere is generally weaker resulting from a more fertile composition, including hydrated minerals, and a higher concentration of heat-producing elements and higher background mantle-related heat flow. This may lead to preferential localization of deformation during regional tectonic events in weaker noncratonic lithosphere. In addition to these nominal contrasts in strength, strain localization along faults and shear zones may lead to significant structural weaknesses.

Structural inheritance relates to mechanical weaknesses in the continental lithosphere that result from previous tectonic events (Erdős et al., 2014; Manatschal et al., 2015; Thomas, 2006). For instance, present-day and preserved ancient collisional orogens are thought to have undergone a subduction-related phase, with the closure of a precursor rift basin. Inversion of precursor basins reuses most of the extensional tectonic structures associated to the basin formation followed by formation of new orogenic contractional structures (e.g., Erdős et al., 2014). Orogenic structural inheritance is expected through weak upper crustal brittle-ductile shear zones rooting in the middle crust and mantle lithospheric shear zones resulting from subduction (Figure 1). Although structural inheritance is widely described in the continental lithosphere, its role in shaping rifted passive margins as well as its relationship with synrift new-formed faults (Figure 1) is still poorly understood.
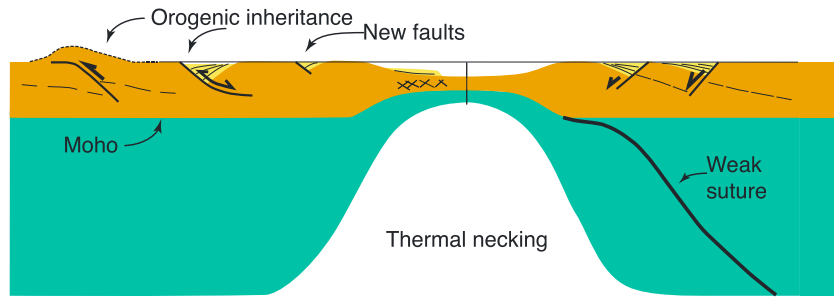
Figure 1. Conceptual diagram illustrating the relationship between tectonic structural inheritance and new-formed shear zones within the context of continental rifting and passive margin formation. Thermal necking is associated with asthenosphere upwelling resulting from continental extension. The weak suture in the lithospheric mantle represents a preserved ancient continental subduction, which may be reactivated during extension.

Tommasi and Vauchez (2001, 2015) suggest that crystallographic lattice preferred orientation of olivine crystals in the lithospheric mantle provided preexisting weakness zones that played a significant role during Mesozoic South Atlantic rifted margin formation. Similarly, correlation of magnetometric and gravimetric mapping of onshore old Pan-African shear zones (Ferreira et al., 2009) and offshore 3-D seismic interpretations (Fetter, 2009) along the Brazilian rifted margin suggest a first-order control of older orogenic structure on the development of the rifted passive margins. However, while the concept of the Wilson cycle is widely accepted, it is not clear how both nominal variations in continental lithospheric rheology and structural inheritance control variations in the structural style of rifts and passive margins.

Previous numerical modeling studies have investigated the role of nominal variations in continental crust rheology, thermal state, and strain rate on the style of rifted margin formation (e.g., Audet & Bürgmann, 2011; Brune et al., 2014; Corti et al., 2007; Dunbar & Sawyer, 1988, 1989; Harry & Sawyer, 1992; Huismans & Beaumont, 2011; Huismans & Beaumont, 2014; Naliboff & Buiter, 2015). Here we present a study of the role of structural inheritance created during extensional and contractional events prior to the development of rifted passive margins by means of high-resolution, plane-strain, thermo-mechanical numerical models. We focus in particular on the role of varying amounts of preorogenic extension and orogenic shortening.

2. Numerical Modeling Method

For the numerical simulations we use a modified highly efficient version of the arbitrary Lagrangian-Eulerian finite element code FANTOM (Erdős et al., 2014; Thieulot, 2011) to model thermal-mechanically coupled, plane-strain, viscous-plastic creeping flows (see also Fullsack, 1995; Willett, 1999). We investigate the behavior of a layered lithosphere and sublithospheric mantle with frictional-plastic and thermally activated power law viscous rheologies in both contractional and extensional regimes.

When stress is below the frictional-plastic yield deformation is viscous and described by temperature-dependent nonlinear power law viscous rheologies based on laboratory measurements. The effective viscosity in the power law rheology is of the following form:

$$\eta_{\text{eff}} = f.A^{-1/n}.\dot{\varepsilon}^{\frac{1-n}{2n}}.\exp\left(\frac{Q + V.p}{nRT}\right),\tag{1}$$

where f is a scaling factor that allows modifying viscous strength without recourse to additional flow laws (Huismans & Beaumont, 2014), A is the preexponential scaling factor, n is the power law exponent, $\dot{\varepsilon}$ is the second invariant of the deviatoric strain rate tensor $\left(\frac{1}{2}\dot{\varepsilon}'_{ij}\dot{\varepsilon}'_{ij}\right)$, Q is activation energy, V is activation volume, p is pressure, T is temperature, and R is the universal gas constant. A, n, Q, and V are derived from laboratorial measurements of *wet* and *dry* olivine (Karato & Wu, 1993) and wet quartz (Gleason & Tullis, 1995) and are given in Table 1.

When stress exceeds the plastic yield criterion, frictional-plastic deformation is modeled by a pressure-dependent Drucker-Prager criterion, which in plane-strain is equivalent to a Coulomb criterion:

Table 1
Input Parameters for the Numerical Models

Units	Décollement layer	Upper crust + precollision sediment	Lower crust	Mantle lithosphere	Sub-lithospheric mantle
	Mechanical parameters				
Thickness (km)	1	21 + 3	10	90	475
Reference density (kg/m^3) ρ_0	2,300	2,800	2,800	3,300	3,300
Internal friction angle ϕ_{eff} (ε)	2°	15°–2°	15°–2°	15°–2°	15°–2°
Strain range of softening	0.05–1.05	0.05–1.05	0.05–1.05	0.05–1.05	0.05–1.05
Cohesion (MPa) C	2	20–4	20–4	20–4	20–4
Flow law	–	Wet quartz	Wet quartz	Dry olivine	Wet olivine
Scaling factor (f)	1	1	100	1	1
A (Pa^{-n}/s)	$8.574 \cdot 10^{-28}$	$8.574 \cdot 10^{-28}$	$8.574 \cdot 10^{-28}$	$2.4168 \cdot 10^{-15}$	$1.393 \cdot 10^{-14}$
Activation energy (J/mol) Q	$222 \cdot 10^3$	$222 \cdot 10^3$	$222 \cdot 10^3$	$540 \cdot 10^3$	$429 \cdot 10^3$
Power law exponent (n)	4	4	4	3.5	3
Activation volume (m^3/mol) V	0	0	0	$25\ 10^{-6}$	$15\ 10^{-6}$
Gas constant (J/mol/C) R	8.1344	8.1344	8.1344	8.1344	8.1344
	Thermal parameters				
Heat capacity (m^2/s^2/K) C$_p$	803	803	803	682	682
Thermal cond. (W/m/K) k	2.25	2.25	2.25	2.25	48.6
Thermal expansion (K^{-1}) α	$3.1 \cdot 10^{-5}$	$3.1 \cdot 10^{-5}$	$3.1 \cdot 10^{-5}$	$3.1 \cdot 10^5$	$3.1 \cdot 10^5$
Heat productivity (W/m^3) A	$0.9 \cdot 10^{-6}$	$0.9 \cdot 10^{-6}$	$0.9 \cdot 10^{-6}$	–	–
Heat flux (mW/m^2)	–	–	–	19.5	19.5
Temperature surface (°C)	–	0	–	–	–
Temperature Moho (°C)	–	–	550	–	–
Temperature base lithosphere (°C)	–	–	–	1,330	–
Temperature base of model (°C)	–	–	–	–	1,520

$$\sigma_y = \left(J_2'\right)^{\frac{1}{2}} = C.\cos\phi_{eff} + p.\sin\phi_{eff}, \tag{2}$$

where J_2' is the second invariant of the deviatoric stress $\left(\frac{1}{2}\sigma_{ij}'\sigma_{ij}'\right)$ and ϕ_{eff} is the effective internal angle of friction given as $p.\sin(\phi_{eff}) = (p - p_f)\sin(\phi)$ for pore fluid pressure p_f and cohesion C. This yield criterion approximates frictional sliding in rocks and the effect of hydrostatic pore fluid pressures. Strain-dependent rheologies allow for the formation of localized frictional-plastic shear zones during lithospheric deformation (Huismans & Beaumont, 2003). In our models strain-softening effects are introduced by a linear decrease of the effective internal angle of friction ϕ_{eff} from 15° to 2°, with a simultaneous decrease of cohesion from 20 to 4 MPa for accumulated strain values between 0.05 and 1.05 (Figure 2). ϕ_{eff} (ε) ~ 15° corresponds to the effective ϕ when the pore fluid pressure is approximately hydrostatic.

The mechanical and thermal systems are coupled through the temperature dependence of viscosity and density and are solved sequentially during each model time step. In what follows, the heat transport equation is solved in two dimensions:

$$\rho.C_p.\left(\frac{\partial T}{\partial t} + v_i\frac{\partial T}{\partial x_i}\right) = \frac{\partial}{\partial x_i}.\left(k\frac{\partial T}{\partial x_i}\right) + H, \tag{3}$$

where ρ is density, C_p is heat capacity, t is time, v_i and x_i are the velocity and spatial components in the i direction, k is thermal conductivity, and H is heat production per unit volume. Density depends on temperature $\rho(T) = \rho_0(1 - \alpha(T - T_0))$, where the thermal expansion coefficient α is 3.1×10^{-5}/°C for the lithosphere and sublithospheric mantle.

2.1. Model Design

The model represents the lithosphere and the sublithospheric mantle in a 1,200-km-wide and 600-km-deep domain (Figure 2). The lithosphere comprises a 35-km-thick continental crust and a 90-km-thick mantle lithosphere. Continental crustal layering is given by a 25-km-thick upper crust and a 10-km-thick lower crust. The upper and lower crusts are wet quartz based (Gleason & Tullis, 1995), but the lower crust is scaled by a factor of 100 to represent strong mafic lower crust. Flow laws for the mantle lithosphere and the sublithospheric mantle are dry and wet olivine (Karato & Wu, 1993), respectively. The upper 4 km of the upper crust are
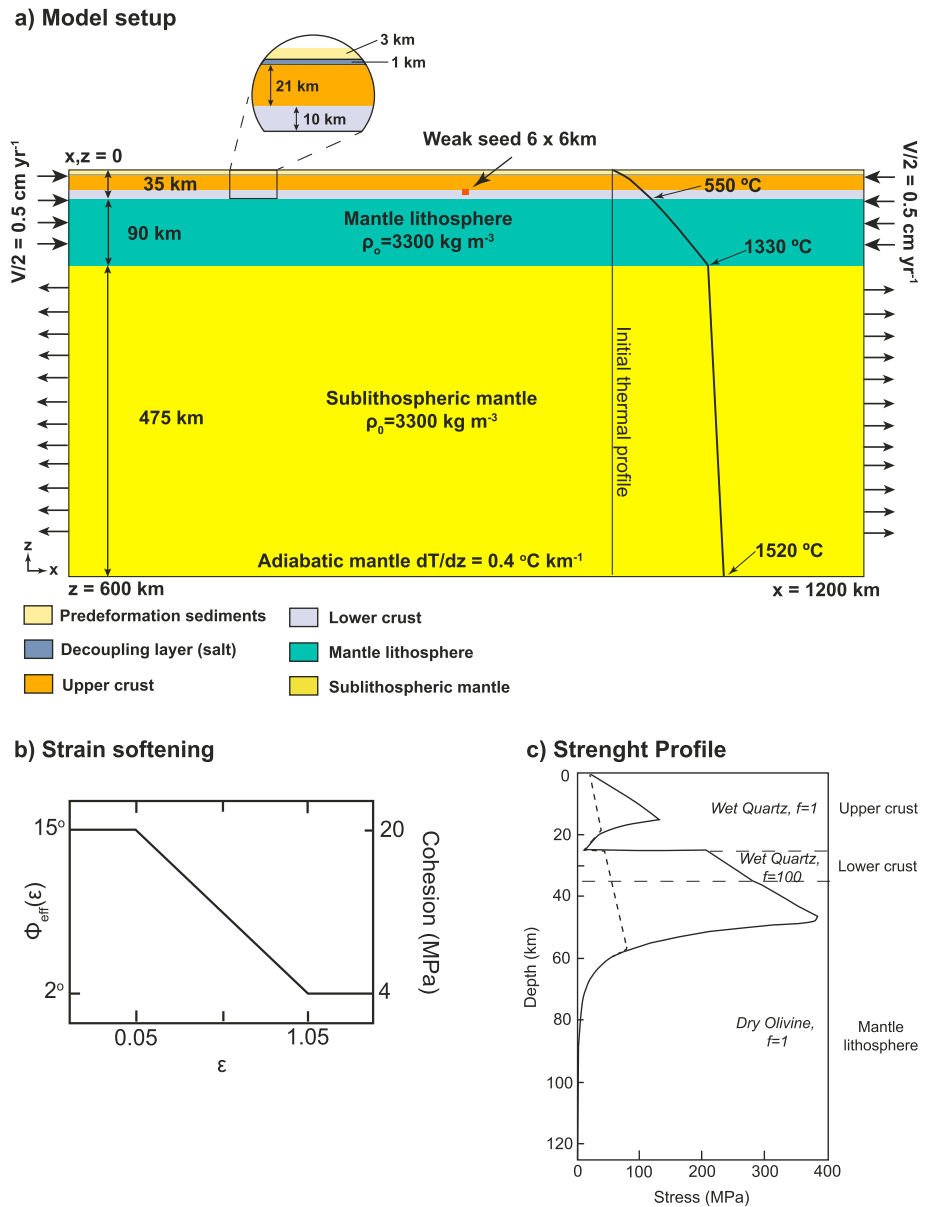
Figure 2. (a) Model design showing the initial layering of the crust, lithosphere, and sublithospheric mantle. Also shown are the initial thermal profile and velocity boundary conditions. All parameters used in the simulations are given in Table 1. The lower part of the figure shows (b) strain softening and the (c) initial stress profile, where the dashed line represents fully strain-weakened lithosphere.

formed by predeformation sediments, with a 3-km-thick frictional upper layer overlying a 1-km-thick weak layer representing a *décollement* horizon. This setup allows for the interaction of both thin- and thick-skinned tectonic deformation. A strain-weakened weak seed of 6 × 6 km is positioned at the top of the lower crust to seed initial localization. The initial conditions are symmetrical, and subduction of the strong lower lithosphere initiates with a random polarity.

The Eulerian grid has 2,400 elements in the horizontal and 300 elements in the vertical dimension, respectively. In the vertical direction, the elements are distributed as 125 for the upper crust, 125 for the lower crust and mantle lithosphere, and 50 elements for the sublithospheric mantle resulting in a vertical resolution of 200 m for the upper crust, 800 m for the lower crust and mantle lithosphere, and 9.5 km for the sublithospheric mantle. The horizontal resolution is 500 m for the entire model. Velocity boundary

Table 2
List of Models and Varying Parameters

Model		Amount of extension (km)	Amount of contraction (km)	Amount of extension (km)	Figure
Two-phase models	M1	–	150	250	Figure 3
	M2	–	300	400	Figure 4
Three-phase models	M3	50	150	250	Figure 5
	M4	50	300	350	Figure 6
	M5	100	300	250	Figure 7
	SM1	100	150	250	SM1
	SM2	50	300	350	SM2
	SM3	100	300	250	SM3
		–	300	400	

conditions applied to the vertical sides of the lithosphere are $V/2 = 0.5$ cm/year, with an influx velocity in the sublithospheric mantle in order to keep the volume in the model domain constant. The upper horizontal boundary is free, whereas the basal horizontal boundary has a free slip condition and zero vertical flow.

The thermal model setup includes lateral boundaries with zero heat flow and constant temperature at upper and lower boundaries. The initial temperature field varies parabolically with depth from the surface ($T_o = 0$ °C) to the Moho ($T_m = 550$ °C) as a result of radioactive heat production in the crust ($h_c = 0.9$ μW/m^3). Below the Moho, temperature follows a linear gradient until the base of the lithosphere ($T = 1330$ °C) and basal heat flux of $q_{ml} = 19.5$ mW/m^2. In the sublithospheric mantle, the temperature gradient is adiabatic until the base of the model, set as $T = 1520$ °C. Thermal conductivity increases linearly to 48.6 W/m/K at 1330 °C in the sublithospheric mantle corresponding to scaling the thermal conductivity by the Nusselt number of upper mantle convection. The enhanced conductivity maintains a constant heat flux to the base of the lithosphere and an adiabatic thermal gradient in the sublithospheric mantle (e.g., Pysklywec & Beaumont, 2004). The model is designed to represent a typical layering of thermally equilibrated Phanerozoic continental lithosphere (Artemieva, 2009; Hawkesworth et al., 2017). The crustal rheological layering with a quartz based upper crust and a strong lower crust is motivated by what is observed in orogens such as the Alps (Schmid et al., 1996; Schmid & Kissling, 2000) and the Pyrenees (Beaumont et al., 2000; Muñoz, 1992), with upper crust about 25 km thick that accommodates most of the upper crustal shortening and a strong lower crust that, based on deep seismic sections, appears to subduct with the mantle lithosphere.

3. Model Results

We explore first the effect of orogenic structural inheritance in model set 1 (M1–M2; Table 2) characterized by two phases, with phase 1 lithosphere shortening followed by phase 2 lithosphere extension. To allow for a broader range of orogenic shear zones model, set 2 (M3–M6; Table 2) exhibits three phases in which the lithosphere shortening is preceded by extension: with phase 1 lithosphere extension, phase 2 shortening, and final phase 3 extension. The models differ by varying amount of prior shortening and extension exploring its effect on rifted margin formation. Supplementary Model 2 (SM2) tests the sensitivity of models to thermal relaxation and strain resetting. SM3 shows how temperature is distributed in models M2 and M5 for the orogenic and rifted margin stages.

3.1. Model Set 1: Contraction-Extension
3.1.1. Model 1: 150-km Contraction Followed by Extension
Model 1 is characterized by 150 km of contraction leading to a small and narrow crustal scale orogen with three deeply rooted thick-skinned thrusts covered by thin-skinned thrust sheets in the prowedge (Figure 3a). Elevation is up to 5 km, whereas the retroforeland basin is 500-m deep and the proforeland basin is 1.5-km deep. During convergence, the first contractional conjugate frictional-plastic shear zones bound a primary pop-up structure (shear zones 1 and 1′), rooted in the weak middle crust (Figure 3a). The mantle lithosphere and strong lower crust exhibit asymmetric subduction, and subsequent thick-skinned crustal basement thrust sheets 2–4 form in sequence in the prowedge toward the foreland.
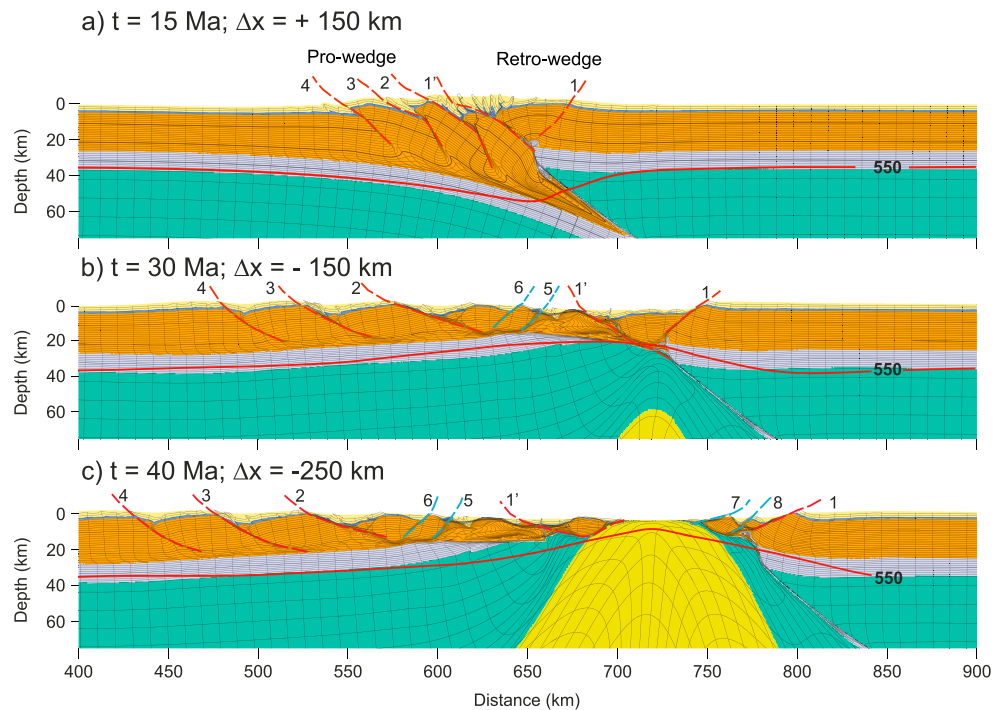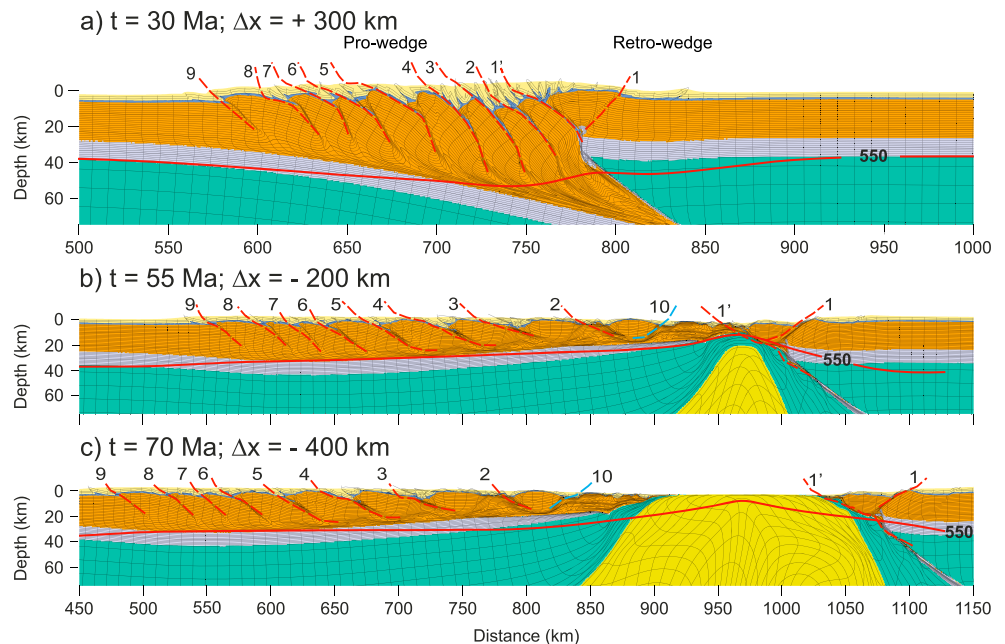
Figure 3. M1. (a) Full orogenic structure after 150 km of contraction, (b) extension of 150 km, and (c) final passive margin configuration after 250 km of extension. The legend for colors is the same as for Figure 2. The dashed lines represent frictional-plastic shear zones, where the red ones are contractional and the blue ones are new-formed extensional shear zones. The numbering represents the chronologic development of shear zones. When shear zones are assigned the same number, they represent simultaneous faulting.

Toward distal parts of the orogen, contraction is accommodated by thin-skinned tectonics. The leading edge of the subducting plate develops a highly ductile wedge of upper crust that is decoupled from the lower crust, which in turn subducts coupled to the mantle lithosphere to 100-km depth. Retrowedge deformation is limited to an incipient shear zone and large-scale upwarping above prowedge subducted mid and lower crust and mantle lithosphere.

In phase 2 velocity boundary conditions are reversed. At t = 30 Ma and after 150 km of extension, the contractional shear zones 1 to 4 are efficiently reused completely reversing the initial contraction (Figure 3b) forming a set of synthetic normal faults, while extension in the mantle lithosphere is localized on the orogenic subduction shear zone. New extensional shear zones 5–6, antithetic with respect to shear zones 1–4, allow exhumation of previously subducted upper continental crust. With continued extension and thinning of the lithospheric mantle, the prowedge crust thins and its lower crust ruptures (Figure 3b). Extensional reactivation in the retrowedge is limited to shear zone 1. With continued extension, deformation in the mantle lithosphere shifts from the orogenic suture zone to a narrow viscous necking zone with upwelling sublithospheric mantle (Figure 3c). New crustal extensional shear zones 7–8 form during final lithosphere breakup attenuating the retrowedge margin (Figure 3c).

The final passive margin architecture is asymmetric with broad crustal extension in the prowedge and narrow extension in the retrowedge side. The distal portion of the wide margin accommodates extension by reactivating contractional shear zones 3 and 4 (Figure 3c). From shear 2 oceanward the necking zone accommodates crustal thinning reusing contractional shear 1 and forming new counter regional shear zones 5 and 6. Within the necking zone, the crust is attenuated from ~30- to 50km thickness with the lower crust being removed toward the most attenuated portion of the margin. The very narrow conjugate *retrowedge* margin is thinned across 50 km through new-formed shear zones 7 and 8, achieving 5 km of thickness. Also, this margin has its lower crust removed, with minor exhumation of mantle lithosphere to the surface and the orogenic suture rooting below the narrow margin.

Figure 4. M2. (a) Full orogenic structure after 300 km of contraction. (b and c) Extension of 200 and 400 km, respectively. Note that structures 6–9 are not reactivated. Color-coding of shear zones is the same as Figure 2.

### 3.1.2. Model 2: 300 km of Contraction Followed by Extension

Model 2 has 300 km of contraction leading to a large asymmetric crustal scale orogen with eight deeply rooted thick-skinned thrusts covered by thin-skinned thrust sheets in the prowedge covered by thin-skinned deformed precollisional sediments on both prowedge and retrowedge (Figure 4a). In the prowedge, contractional shear zones 1 to 9 form in sequence. In the retrowedge, contractional shear 1 is more developed in comparison with Model M1, with one thin-skinned thrust sheet toward the foreland. The lower crust subducts along with the mantle lithosphere to 150-km depth as in model M1.

Phase 2 rifted passive margin formation leads, similarly to model M1, to narrow localization along the orogenic mantle lithospheric shear zone and broad distributed extensional deformation within the crust, with a broad domain of crustal extension on the former prowedge side and a very narrow extensional domain in the retrowedge margin (Figures 4b and 4c). One of the main differences with respect to model M1 is that not all prowedge orogenic shear zones are reactivated. Shear zones 1 to 4 proximal to the necking zone are fully reactivated, while distant orogenic shear zones 5 to 9 are not, resulting in preservation of the orogenic structure in the proximal domain of the rifted margin system (Figures 4b and 4c). Previously, subducted upper crust is exhumed to shallow crustal levels through extensional reactivation of shear zones 2–4 and new-formed extensional shear 10. The conjugate retrowedge margin accommodated extension with the reactivation of the previously contractional shear zones 1′, without formation of new extensional shear zones resulting in a very narrow necking zone (Figure 4c). Lower crust is removed on both conjugate margins. The orogenic suture zone roots similarly to model M1 under the retrowedge margin, leaving tracts of lower crust in the mantle lithosphere.

3.2. Model Set 2: Extension-Contraction-Extension
3.2.1. Model 3: 50-km Extension, 150-km Contraction, Followed by Extension

Model 3 is characterized by a first phase of 50 km of extension, followed by 150 km of contraction and subsequent extension. Initial moderate rifting leads to a small symmetric continental rift basin with two main conjugate extensional shear zones rooting in the strong lower crust and upper mantle lithosphere (Figure 5a). The lower crust is completely removed from the base of the graben. The central domain of the graben exhibits a second set of smaller scale conjugate normal shear zones (Figure 5a). During contraction phase 2, conjugate shear zones 2 first reactivate and invert followed by shear zones 1, developing a doubly vergent pop-up structure transported onto the retrowedge (Figure 5b). Further shortening leads to outward
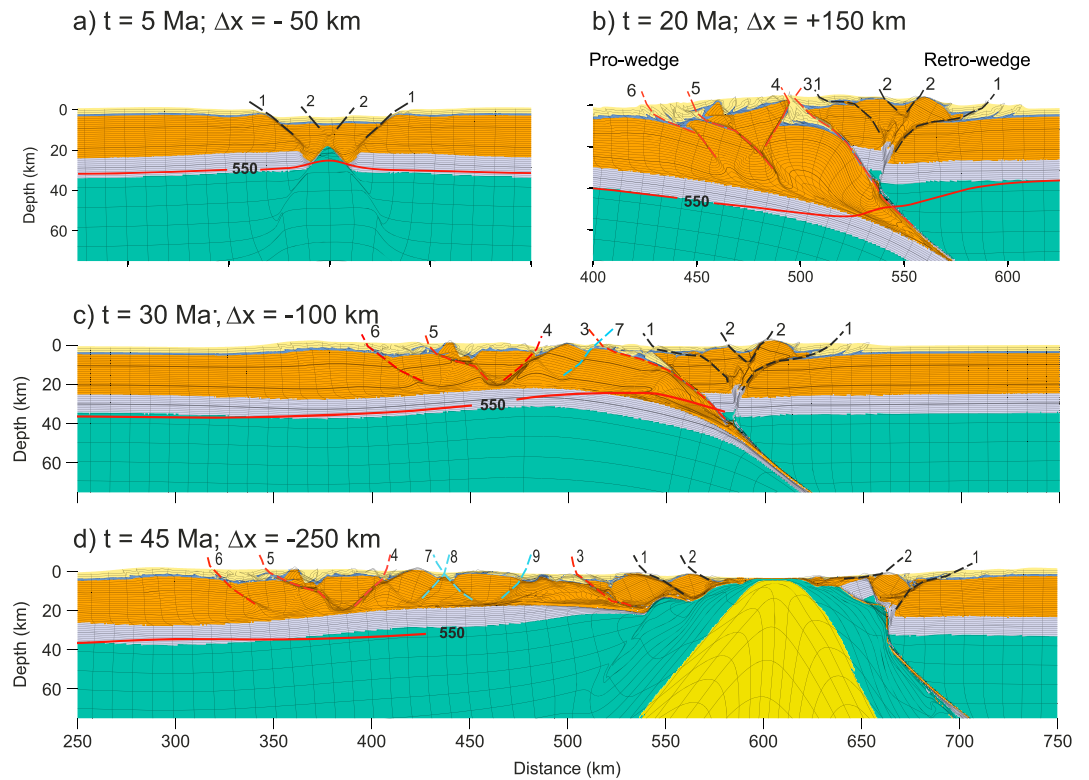
Figure 5. M3. (a) About 50 km of preorogenic extension showing simultaneous faulting during the development of preorogenic extensional shear zones (black dashed lines). (b) Full orogenic structure after 150 km of contraction. (c) Continued extension (100 km) and development of new-formed extensional structure 7 in the prowedge. (d) Final passive margin configuration and crustal breakup following inherited extensional shear zones in the retrowedge.

propagating thick-skinned basement thrusts sheets in the prowedge and subduction of the continental mantle lithosphere at depth. At the surface thin-skinned thrusting affects precollision sediments on both prowedge and retrowedge (Figure 5b). The resulting doubly vergent orogen has two main thick-skinned thrust sheets bounded by new contractional shear zones 3 to 6. The retrowedge is much more structured in comparison with models M1 and M2 with pure contraction and controlled by reactivation of previously developed extensional shear zones. The subducting plate also develops a highly ductile wedge of upper continental crust that subducts along with the lower crust.

In phase 3 the boundary conditions are reversed to extension. The mantle lithospheric suture zone initially localizes strain quite efficiently. Within the crust strain localizes in the central domain of the orogen, whereas the prowedge orogenic shear zones are efficiently reused during extension (Figure 5c). Extensional shears 7 to 9 develop as a result of exhumation of previously deeply buried continental crust and represent the transition from extension to thinning. Thermal weakening and upwelling of the sublithospheric mantle cause the orogenic suture to be abandoned and result in extensional reactivation of retrowedge shear zones 1 and 2 (Figure 5d). The final rifted passive margin configuration (Figure 5d) is asymmetric, with a wide *prowedge* margin and a narrow retrowedge margin. The structure of the proximal wide margin is controlled by orogenic inherited shear zones 4 to 6. The necking zone, ocean ward from shear 4, accommodates extension on reactivating long-lived orogenic and prior extension shear zones and on new-formed extensional shear zones 7 to 9 in the distal margin (Figure 5d). The conjugate narrow rifted margin resulting from extension of the former orogenic retrowedge reuses inherited extensional shear zones 2 from phase 1 (Figure 5d) and exhumes lower crust to very shallow crustal levels. Both sides of the final rifted conjugate passive margin exhibit minor exhumation of mantle lithosphere in the ocean continent transition zone.

3.2.2. Model 4: 50-km Extension, 300-km Contraction, Followed by Extension
Model 4 is characterized by a first phase of 50 km of extension, followed by 300 km of contraction and subsequent extension. Phase 1 extension and early phase 2 contraction are the same as in Model 3. The
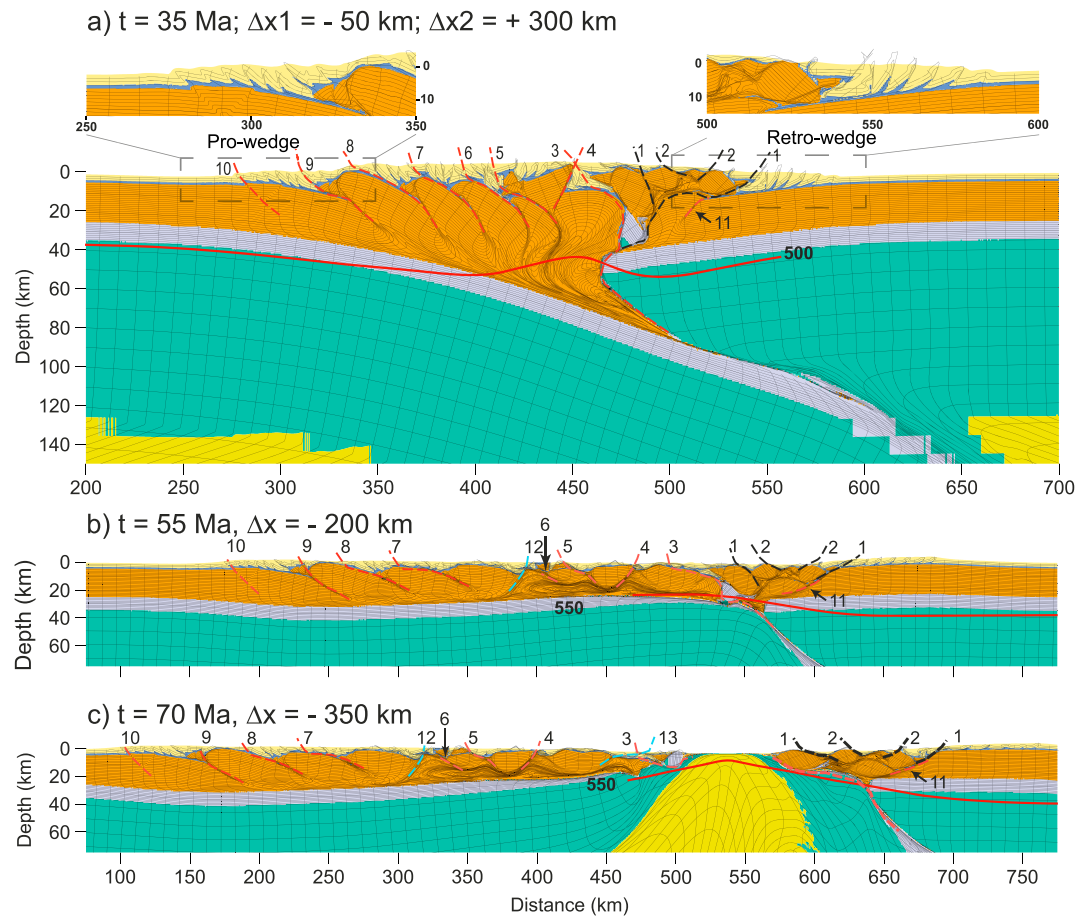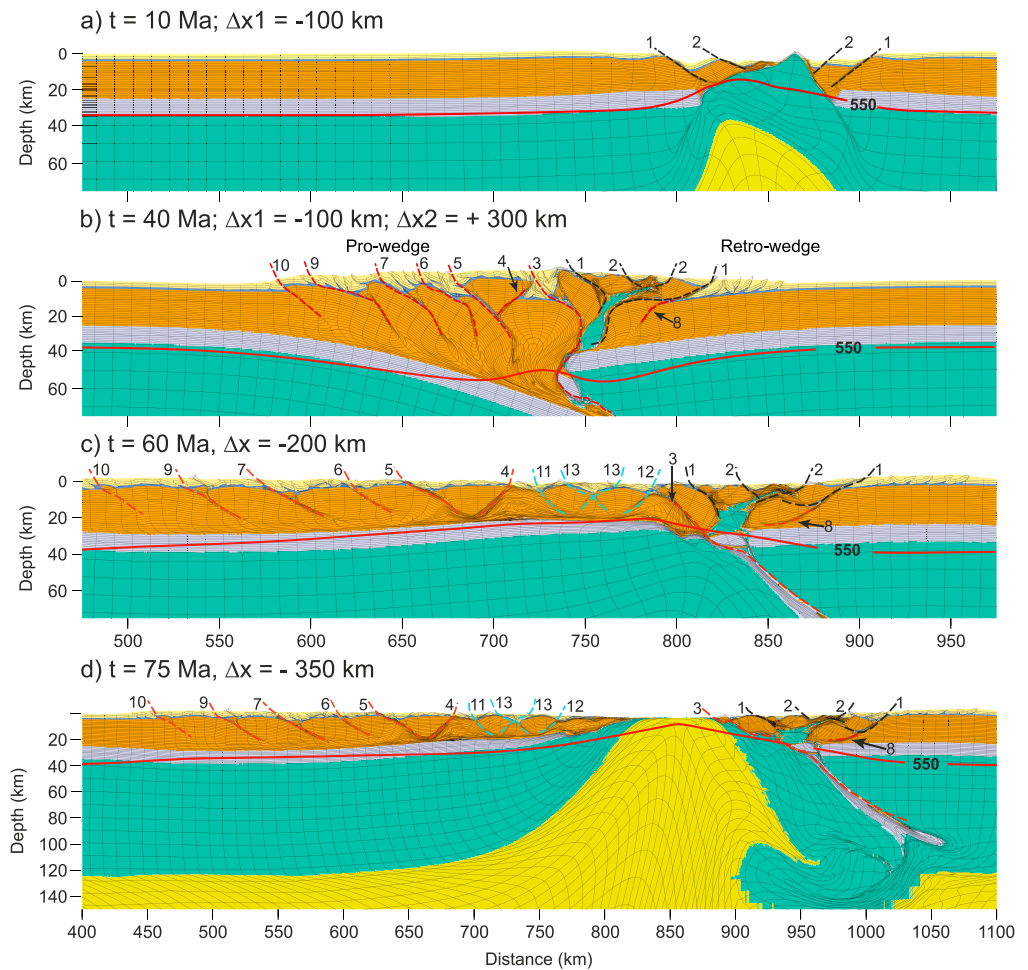
Figure 6. M4. (a) Full orogenic structure after inversion of 50 km of preorogenic extension plus 300 km of contraction. Insets show thin-skin deformation in the forelands. (b) Extension of 200 km in phase 3. Full reactivation of all contractional shear zones in the prowedge and development of new-formed extensional structure 12. (c) Final passive margin configuration. Note that crustal breakup did not follow neither inherited nor new-formed shear zones. Instead, it followed the contact between tracts of lower crust with the upper crust.

orogenic configuration at $t = 35$ Ma and 300 km of contraction exhibits six thick-skinned thrusts (bounded by shear zones 3 to 10) covered by thin-skinned deformed precollisional sediments in the prowedge (Figure 6a). Below the prowedge, ductile upper continental crust is subducted to 90-km depth. Inverted extensional shear zones 1 and 2 structure the retrowedge.

During phase 3 at 55 Ma and 200 km of extension, shear zones 1 to 6 and 11 are fully reactivated accommodating extension, whereas shear zones 7 to 10 do not reactivate and preserve part of the orogenic structure (Figure 6b). Extensional reactivation of prowedge shear zones 3 to 6 exhumes upper continental crust previously subducted to large depths. Retrowedge shear zones 1, 2, and 11 accommodated extension in the retrowedge, with new shear 11 transporting phase 1 shear zones 1 and 2 to the rifted margin. Breakup occurs after about 70 Ma and 350 km of extension. The orogenic suture zone with remnants of lower continental crust roots below the extended retrowedge margin (Figure 6c). The resulting conjugate rifted passive margin (Figure 6c) is highly asymmetric. The former prowedge develops into a very wide and complexly structured passive margin, ~400-km long. Its proximal domain is controlled by inherited contractional shear zones, which were not efficiently reactivated, preserving orogenic thick- and thin-skinned structures. The intermediate and distal margin show interplay between inherited contractional and extensional shear zones, resulting in extension and thinning of the continental crust from ~40 to <5 km in the distal margin. A small block of lower continental crust originating from the orogenic retrowedge exhumes in the ocean-continent transition zone. The very narrow conjugate retrowedge passive margin is mostly extended by reactivation of inherited extensional and contractional shear zones.

Figure 7. M5. (a) About 100 km of preorogenic extension showing two conjugate sets of extensional faults and crustal breakup. (b) Full orogenic structure after 100 km of preorogenic extension plus 300 km of contraction. (c) After 200 km of extension, the prowedge shows fully and unreactivated (7–9) contractional shear zones and development of new-formed extensional shear zones sequentially (11 and 12) and later simultaneously (13). (d) In the retrowedge, extension occurs with the interplay between inherited extensional (1) and contractional (8) shear zones to form a main border fault of the rifted passive margin.

3.2.3. Model 5: 100-km Extension, 300-km Contraction, Followed by Extension

Model 5 and SM1 test the effect of larger phase 1 extension leading to lithospheric breakup on subsequent phase 2 orogenic structure and phase 3 rifted margin formation. At t = 10 Ma and 100 km of extension the crust has fully ruptured along conjugate extensional shear zones 1 and 2 leading to exhumation of mantle lithosphere to the surface (Figure 7a). Phase 2 orogenic structure after 300-km shortening is similar to Model M4 with five basement thrust sheets in the prowedge and inversion of the crustal extensional shear zones in a pop-up structure in the retrowedge margin. The main difference with respect to Model 4 is the incorporation of a large fragment of mantle lithosphere in the inversion structure in the retrowedge at a very shallow crustal level (Figure 7b).

During phase 3 extension (Figures 7b and 7c), extensional reactivation occurs on shear zones proximal to the mantle lithospheric necking zone, similar to the previous models. As the prowedge is educted, extension is accommodated first by reactivation of contractional shear zones 4 to 10 in the proximal domain of the developing wide margin (Figure 7c). With continued extension, new extensional shear zones 11 to 13 form when the deeply buried basement thrust 5 exhumes to the surface. Strain accumulation migrates to the necking zone of the evolving margin, preserving the orogenic structure (contractional shear zones 4 to 10) and crustal thicknesses in the proximal margin (Figure 7b). The final rifted passive margin configuration is,
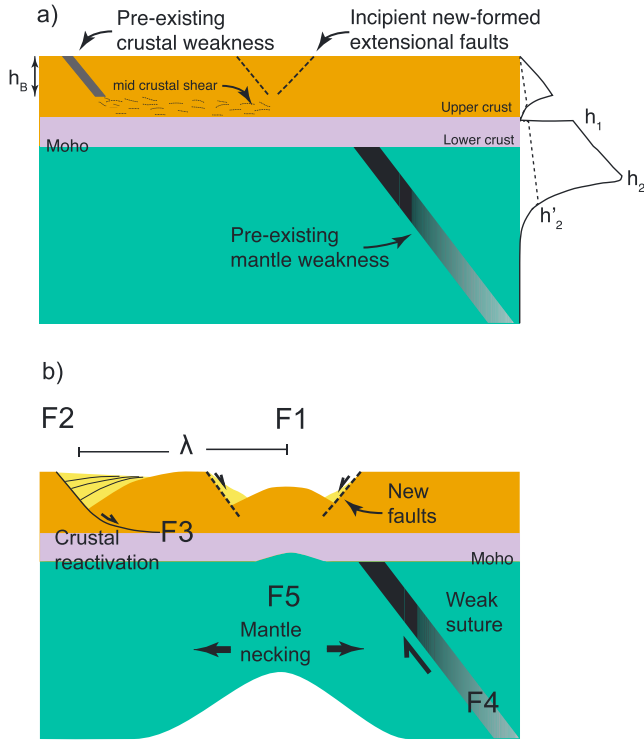
Figure 8. Conceptual illustration for the dynamic analysis. (a) Preexisting upper crustal and mantle lithospheric weaknesses, new-formed upper crustal extensional faults, midcrustal shear zone linking offset weak preexisting upper crustal faults and necking area, and continental lithosphere strength profile (right side). (b) The different domains F1–F3 in the crust and its relation to λ and F4–F5 in the mantle lithosphere.

as in previous models, asymmetric with a 400-km-wide prowedge margin and a 150-km-wide retrowedge margin (Figure 7d). Inherited orogenic shear zones control the proximal prowedge margin. The necking zone is characterized by crustal thinning from 35 km to less than 5 km over a distance of about 175 km. The narrow retrowedge margin is thinned from its original thickness to the OCT over 150 km with fragments of mantle lithosphere as shallow as 5 km in the extended crust (Figure 7d). Both margins exhibit a minor area of exhumed mantle lithosphere between the edge of the continental crust and new *oceanic* lithosphere.

4. Dynamic Analysis of Inheritance Reactivation

We next quantify the role of orogenic inheritance within the upper crust and mantle lithosphere. A force balance analysis is used to predict (1) the length scale over which reactivation of weak inherited upper crustal structure offset from the necking zone may occur and (2) the competition between reactivation of the weak mantle lithospheric suture zone and extensional necking of the mantle lithosphere in the rift area.

For the analysis of reactivation of offset orogenic weak zones we compare the contrast in integrated strength F1 of the frictional-plastic upper crust for a domain without inheritance in the necking area (Figure 8) and balance this with the force needed to reactivate an offset weak frictional-plastic upper crustal shear zone, F2, and the integrated viscous resistance F3 on the weak viscous middle crust (e.g., Braun & Beaumont, 1989):

$$F_1 = \int_0^{h_b} \rho_c.g.z. \sin(\phi_s)dz = \rho_c.g.\frac{h_b^2}{2}. \sin(\phi_s) \qquad (4)$$

and

$$F_2 = \int_0^{h_b} \rho_c.g.z. \sin(\phi_w)dz = \rho_c.g.\frac{h_b^2}{2}. \sin(\phi_w) \qquad (5)$$

where ρ_c is crustal density, g is acceleration due to gravity, z is depth, ϕ_s is the internal angle of friction, and ϕ_w is the internal angle of friction for weakened domains, and integration is from the surface at $z = 0$ to the base of the frictional-plastic upper crust at $z = h_b$ (see the supporting information for detailed formulations). Domain F2 is where new faults are likely to develop and the connection between inherited and new-formed structures is given by a low-angle midcrust shear zone. Integrated strength in the midcrust shear (F3) is given as a function of viscosity (μ_c) and strain rate ($\dot{\varepsilon}$) over the length (λ) of this shear zone (Figure 8b). Here we assume a constant linear viscosity along the weak mid crust *décollement*. In order for reactivation of inherited structures to occur the combined strength of weak inherited structures F2 and the resistance to sliding along the weak mid crust F3 should be less or equal that of the force required for formation of new structures F1. Using that F1 = F2 + F3, we can extract the maximum length scale λ over which offset weak inherited structures can reactivate:

$$\lambda = \frac{\rho_c.g.h_b^2(\sin(\phi_s) - \sin(\phi_w))}{2\mu_c\dot{\varepsilon}}. \qquad (6)$$

The maximum length for reactivation λ is controlled by the frictional-plastic strength contrast between F1 and F2 and inversely by the viscous resistance in F3, where λ is inversely related to midcrustal viscosity (Figure 9a). This prediction matches well with results shown in the numerical models above that are characterized by an effective viscosity 1.9×10^{20} Pas for the midcrustal *décollement* and a strain rate of 0.3×10^{-13}/s, predicting maximum offset at λ ∼ 120 km. The models presented exhibit reactivation for
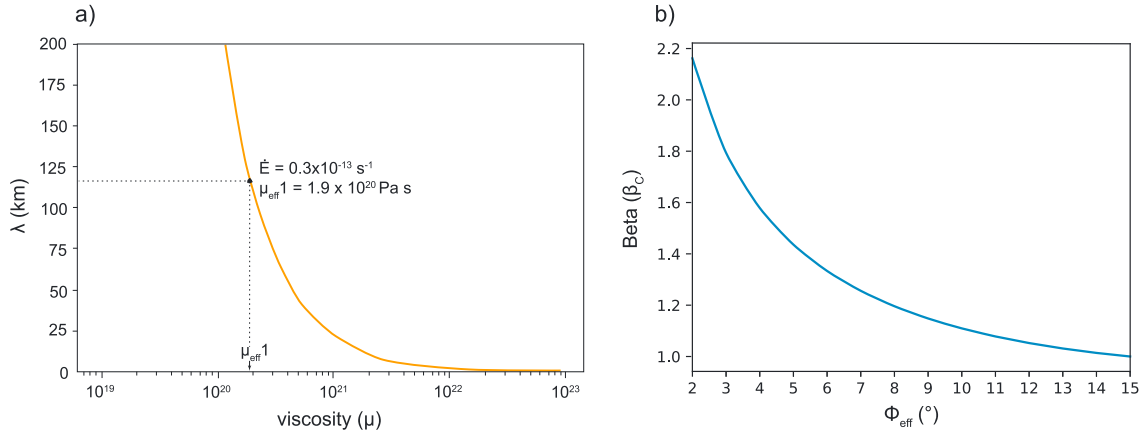
Figure 9. (a) Inverse relation between λ and midcrust viscosity. Note characteristic offset λ = 120 km for conditions consistent with numerical models. (b) Relation between the frictional strength of the suture zone and the critical thinning factor β_c. When healing of the frictional shear occurs, we expect the effective frictional angle of the suture to increase from its weakened value ϕ_w = 2° to the reference strong frictional angle ϕ_s = 15°.

offsets <100 km and minor to no reactivation for structures at larger distance from the necking area. With a thicker midcrustal *décollement*, the shear strain rate will be lower given the same kinematic conditions, which will allow for reactivation over a larger distance. In contrast with increasing strain rate the flow stress in the viscous shear zone increases, with an expected corresponding decrease in λ (see equation (6)).

To analyze the competition between reactivation of the weak lithospheric suture zone and extensional necking of the mantle lithosphere, we compare the integrated strength of the weak suture zone F4 and the strength of the pristine upper mantle lithosphere F5 that is undergoing thinning by a factor β (e.g., Figure 8b):

$$F_4 = \int_{h_1}^{h'_2} \rho_m . g . z . \sin(\phi_w) dz = \rho_m . g . \sin(\phi_w) . \left(\left(h'_2 \right)^2 - (h_1)^2 \right) \tag{7}$$

and

$$F_5 = \int_{h_1/\beta}^{h_2/\beta} \rho_m . g . z . \sin(\phi_s) dz = \frac{\rho_m . g}{2} . \sin(\phi_s) . \left(\left(\frac{h_2}{\beta} \right)^2 - \left(\frac{h_1}{\beta} \right)^2 \right) \tag{8}$$

where h_1 = 25 km is the depth to the upper part of the strong lower crust, h_2 = 60 km is the depth to the base of the strong not strain weakened frictional-plastic mantle lithosphere in the necking area with unweakened coefficient of friction ϕ_s = 15°, h'_2 = 50 km is the depth to the base of the strain weakened frictional-plastic mantle lithosphere in the suture zone with weakened coefficient of friction ϕ_w, β is the thinning factor, and ρ_m is the density of the mantle lithosphere.

The critical mantle lithospheric thinning factor β_c at which the necking area has the same strength as the mantle suture zone is expected when F4 = F5, assuming differences in viscous strength between suture zone and necking area are negligible (e.g., Naliboff & Buiter, 2015). For thinning factors $\beta > \beta_c$ the suture is expected to be deactivated. The critical thinning factor β_c is given by (see the supporting information for details):

$$\beta_c = \sqrt{\frac{\sin \phi_s}{\sin \phi_w} . \frac{(h_2{}^2 - h_1{}^2)}{(h'_2{}^2 - h_1{}^2)}} \tag{9}$$

For the parameters used in the models with ϕ_s = 15° and ϕ_w = 2° this relation predicts that mantle lithospheric necking will dominate for $\beta > 2.2$, consistent with our results. We can also use this relationship to consider how mechanical healing of the suture zone may affect the critical thinning factor β_c. When

healing of the frictional-plastic shear zone occurs, we expect the effective frictional angle of the suture zone to increase from its weakened value $\phi_w = 2°$ to the reference strong frictional angle $\phi_s = 15°$. We can therefore interpret the horizontal axis (Figure 9b) as the degree of weakening from 0 to 100% with a healing factor τ_h varying between (0 and 1). Consequently, for full fault healing with suture strength defined by $\phi_{eff} = 15°$ necking will dominate from the start of extension (e.g., at $\beta = 1$).

5. Discussion

5.1. Role of Structural Inheritance on Rifted Margin Style

All models show similar general characteristics: (1) initial subduction of the continental lithosphere during the contractional phase; (2) decoupling of the upper and lower continental crust with subduction of lower crust with the mantle lithosphere and formation of an upper crustal orogenic wedge; (3) growth of the prowedge by asymmetric orogenic accretion in case of pure contractional models; (4) when a precursor extensional phase 1 is added to the model, inherited extensional structures permit the migration of deformation to the orogenic retrowedge, resulting in a more symmetric orogenic style in contractional phase 2; (5) deformation during phase 3 extension is highly localized in the mantle lithosphere as a result of the weak orogenic suture zone; and (6) decoupling in the mid crust and distributed extension of the orogenic wedge by reactivation of weak upper crustal shear zones.

5.2. Factors Controlling the Reactivation of Structural Inheritance

We identify four primary factors that control the structural style of rifted margin formation in the presence of orogenic structural inheritance. (1) The strength of orogenic shear zones in the upper crust and upper mantle lithosphere, which in the models is controlled by strain weakening. The single weak mantle lithospheric orogenic suture zone exerts a main control on margin structure by highly efficient localization of extensional deformation upon reactivation. Multiple weak upper crustal orogenic shear zones control extensional basin and rifted margin structure. (2) The degree of decoupling between upper crust and the strong lower crust-lithospheric mantle layer, which controls the distance over which the highly localized strain in the weak mantle suture zone can connect with offset weakness zones in the upper crust (e.g., Braun & Beaumont, 1989). (3) The amount of shortening and size of the orogen. More orogenic shortening leads to larger offset between the weak mantle shear zone and offset weaknesses in the upper crust and reduced potential for reactivation of crustal orogenic shear zones in a position distal to the suture zone. (4) Preorogenic extensional inheritance, which provides a primary control on orogenic structure by reducing orogenic asymmetry and promoting retrowedge shortening. As a result the distribution of orogenic structural weakness in the upper crust is more symmetric with respect to the underlying orogenic suture zone, which in turn results in a more symmetric margin structure.

During the development of phase 3 rifted margin formation, extensional shear zones inherited from phase 1 and used during contractional phase 2, reactivated to accommodate stretching in the retrowedge, whereas contractional inherited shear zones control prowedge stretching. All three-phase models form new extensional shear zones in the prowedge with continued rifting, and models with a lower amount of contraction during phase 2 result in more new-formed structures as compared with models with larger amounts of shortening. This is because models with a lower amount of precursor contraction leave larger domains without orogenic structure and a greater propensity for formation strain-weakened shear zones.

We show using a force balance analysis that the effective viscosity of the midcrustal detachment controls the maximum length over which offset upper crustal weaknesses related to orogenic structural inheritance can reactivate, consistent with earlier results by Braun and Beaumont (1989). For a nominal wet quartz-based rheology (e.g., Gleason & Tullis, 1995), typical midcrustal temperature of ~500 °C, and strain rate of 10^{-13}/s (Pfiffner & Ramsay, 1982) the analysis predicts a maximum length scale over which reactivation may occur in the order $\lambda = 100$ km. The models and force balance analysis presented here show that structural inheritance in the mantle lithosphere related to the ancient subduction zone may play an important role during extensional reactivation, provided mechanical healing plays a limited role. During passive margin formation, suture reactivation and mantle lithosphere necking compete in accommodating lithosphere extension. Progressive thinning and weakening of the necking zone result in abandonment of the suture zone. The force balance analysis presented above predicts that the

critical thinning factor at which mantle lithospheric necking will dominate given the strain-weakened strength of the suture zone, for a shear zone without mechanical healing and parameters used here, is $\beta_c = 2.2$.

5.3. Model Limitations

Here we have focused on the role of orogenic structural inheritance on the structural style of rifted margin formation. The models presented here are by no means exhaustive, and a number of other factors that influence the configuration of rifted passive margins, such as variations in rheological, compositional, and thermal structure investigated in earlier studies (e.g., Huismans & Beaumont, 2011, 2014), are not included here. Models shown in this study represent moderately strong lower crust. We have tested the effect of a 100 Myr long phase of thermal relaxation following orogenic shortening in combination with strain healing for temperatures larger the 450 °C (see SM2). Model SM2 shows that the results are not very sensitive to both these effects. The existence and distribution of weak frictional shear zones in the upper crust and the weak upper crustal material in the suture zone largely control reactivation. Furthermore, our numerical models are 2-D, and any 3-D effects such as obliquity between the rift extension direction and preexisting basement structure, which may play an important role during reactivation (e.g., Fossen et al., 2016), are not included here.

5.4. Comparison to Natural Systems

We next compare model results with observations from two natural systems: a transect through South Norway with inherited Caledonian structure and the Mesozoic North Sea rift (Christiansson et al., 2000; Fichler et al., 2011), and a conjugate margin transect in the South Atlantic with the Brazilian Espírito Santo (Blaich et al., 2011; Zalán et al., 2011) and West African Kwanza (Blaich et al., 2011; Hudec & Jackson, 2004) rifted margins with the onshore inherited Pan-African orogenic structure of the Araçuaí (Pedrosa-Soares et al., 2001; Wiedemann et al., 2002) and Congo (Tack et al., 2001) orogens. Three characteristic domains predicted by the forward models can be recognized in both natural systems: domain A with nonreactivated orogenic structure in a very distal position with respect to the main locus of extension, an intermediate domain B with partial reactivation of orogenic structure, and a domain C at the main locus of extensional basin formation with a combination of reactivated and new-formed extensional structures.

In the Norwegian example (Figure 10a), domain A comprises nonreactivated inherited contractional structure with continental margin units thrust toward the east on top of autochtonous Baltica basement, the Caledonian front in the Oslo area (Fossen et al., 2014). Domain B exhibits a combination of extensional reactivation of the basal Caledonian thrust zone, subsequent formation of new extensional shear zones, and progressive thinning of the crust. Domain C is the North Sea rift area with demonstrated orogenic inheritance in early rift normal faults and the location of the postulated Caledonide suture zone at depth under the North Sea rift basin (e.g., Fossen et al., 2016). The tectonic evolution of domains A–C supports an important role for Caledonian orogenic inheritance on postcollisional extension and rift basin formation (Fossen, 2010). The transition from unreactivated domain A to domain C with new-formed structures occurs over the width of domain B, which is ~100 km and consistent with model predictions.

The second example is between Brazil and Africa, in the Central South Atlantic (Figure 10b). Orogenic structural inheritance is represented by the Pan-African Araçuaí Orogen in the Brazilian margin (Wiedemann et al., 2002) and by the West Congo Orogen in African counterpart (Tack et al., 2001). In both margins, domain A is represented by the Pan-African Araçuaí orogen in East Brazil and the Congo orogen in West Africa (Tack et al., 2001; Wiedemann et al., 2002). The Pan-African orogenic structure was reactivated by early postcollisional extension that most likely restored the crust to close to its present-day thickness of between 35 and 40 km (Bento dos Santos et al., 2015) but remained stable during Mesozoic rifting and passive margin formation. While there is no documented evidence for a role of orogenic inheritance, our model predictions allow the interpretation of a domain B where crustal thicknesses decrease to ~25 km accommodated by the reactivation of orogenic structures and initial development of new-formed extensional shear zones (Figure 10b) with crustal thicknesses of ~25 km. The distal margin is likely controlled by a combination of inherited and new structures and is therefore considered Domain C.
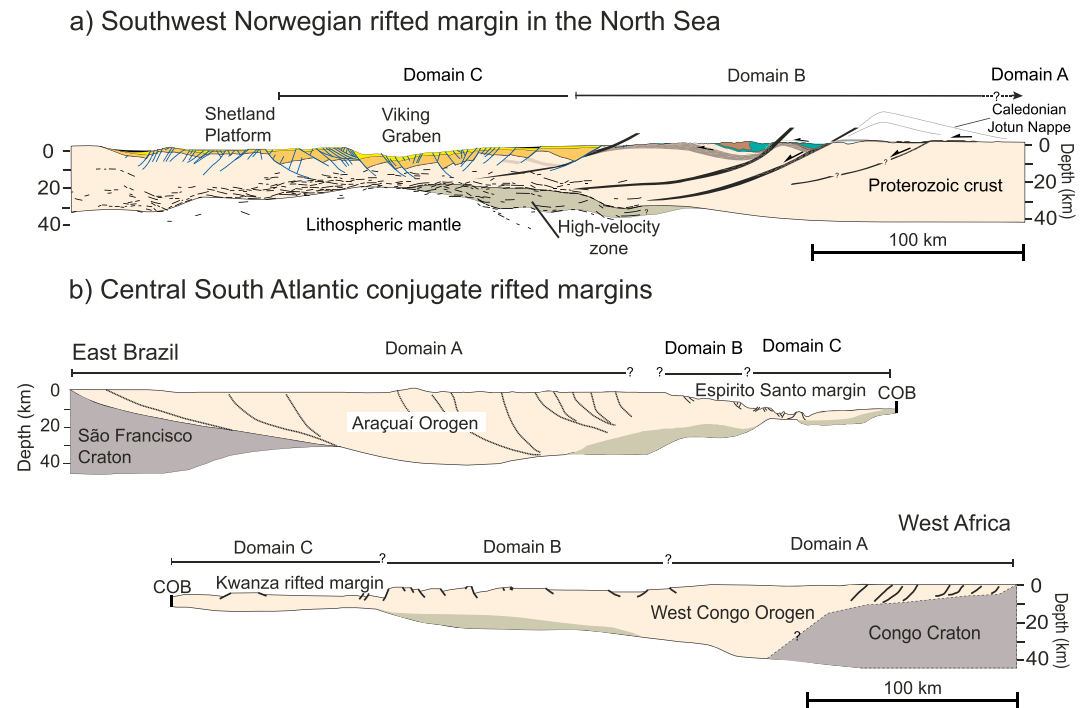
Figure 10. (a) Present-day rifted margin in Southwest Norway, North Sea. The offshore (domain C) part of this transection was interpreted by Christiansson et al. (2000) and Fichler et al. (2011) through deep seismic reflection and refraction data plus gravity and magnetic data. Onshore part mostly following Fossen (1992). Note that beneath the high-velocity zone there are east dipping mantle reflections. (b) Present-day rifted conjugate sections in the Central South Atlantic between Brazil and Africa. Upper section shows Brazilian passive margin with the Espírito Santo Basin and its Araçuaí Orogen onshore connection. Onshore geology was interpreted following gravity-based geological sections of Wiedemann et al. (2002), and offshore crustal structure was interpreted after seismic sections of Blaich et al. (2011) and Zalán et al. (2011). Lower section shows the African conjugate with the Kwanza Basin and the West Congo Orogen onshore connection. Onshore geology was interpreted after geological type cross sections of (Tack et al., 2001), and offshore crustal structure was interpreted after seismic sections of Blaich et al. (2011), structural maps by Guiraud et al. (2010), regional transect made by Hudec and Jackson (2004), and gravimetric modeling by von Nicolai et al. (2013). See text for explanations of domains A-C.

6. Conclusions

In this paper we used self-consistent forward thermo-mechanical numerical models to explore how structural inheritance affects the development and structural style of conjugate rifted passive margins. We conclude the following:

1. The primary factors that control the structural style of conjugate rifted margin formation in the presence of orogenic structural inheritance are the following: (i) the strength of orogenic shear zones in the upper crust and upper mantle lithosphere, (ii) the degree of decoupling between upper crust and the strong lower crust-lithospheric mantle layer, (iii) the amount of shortening and size of the orogen, and (iv) the role of preorogenic extensional inheritance on orogenic wedge structure.
2. The offset between the weak mantle lithospheric orogenic suture zone and orogenic upper crustal weakness zones and the strength of the midcrustal decoupling horizon are the main controlling factors for extensional reactivation. Force balance analysis shows that the maximum length for reactivation λ is controlled by the frictional-plastic strength contrast and is inversely related to the viscous resistance of the midcrustal *décollement*.
3. During passive margin formation, suture reactivation and mantle lithosphere necking compete in accommodating lithosphere extension. Progressive thinning and weakening of the necking zone result in abandonment of the suture zone. Force balance analysis predicts that the critical thinning factor at which mantle lithospheric necking will dominate given the strain-weakened strength of the suture zone, for a shear zone without mechanical healing and parameters used here, is $\beta_c \sim 2.2$.

4. With a small amount of contraction, thick-skinned thrusts are efficiently reactivated in extension, whereas with larger amounts of contraction, thick-skinned thrusts distal to the mantle lithospheric suture zone remain unreactivated.

5. During the extension of the prowedge, reactivation of inherited contractional structures prevails, whereas the extension of the retrowedge is mainly controlled by phase 1 inherited extensional structures. Systems with structured retrowedges guide strain localization and concentrate crustal breakup upon extension.

6. Small amounts of precursor extension and contraction result in less inherited structures and promote formation of new-formed extensional shear zones during phase 3 extension.

7. Models presented here provide insights into the role of orogenic inheritance and its reactivation during subsequent extension in natural systems such as South Norway Caledonides, North Sea Viking Graben, and Central South Atlantic.

References

Artemieva, I. M. (2009). The continental lithosphere: Reconciling thermal, seismic, and petrologic data. *Lithos*, *109*(1–2), 23–46. https://doi.org/10.1016/j.lithos.2008.09.015

Audet, P., & Bürgmann, R. (2011). Dominant role of tectonic inheritance in supercontinent cycles. *Nature Geoscience*, *4*(3), 184–187. https://doi.org/10.1038/ngeo1080

Beaumont, C., Muñoz, J. A., Hamilton, J., & Fullsack, P. (2000). Factors controlling the Alpine evolution of the Central Pyrenees inferred from a comparison of observations and geodynamical models. *Journal of Geophysical Research*, *105*, 8121–8145. https://doi.org/10.1029/1999JB900390

Bento dos Santos, T. M., Tassinari, C. C. G., & Fonseca, P. E. (2015). Diachronic collision, slab break-off and long-term high thermal flux in the Brasiliano–Pan-African orogeny: Implications for the geodynamic evolution of the Mantiqueira Province. *Precambrian Research*, *260*, 1–22. https://doi.org/10.1016/j.precamres.2014.12.018

Blaich, O. A., Faleide, J. I., & Tsikalas, F. (2011). Crustal breakup and continent-ocean transition at South Atlantic conjugate margins. *Journal of Geophysical Research*, *116*, B01402. https://doi.org/10.1029/2010JB007686

Braun, J., & Beaumont, C. (1989). Dynamical models of the role of crustal shear zones in asymmetric continental extension. *Earth and Planetary Science Letters*, *93*(3–4), 405–423. https://doi.org/10.1016/0012-821X(89)90039-3

Brune, S., Heine, C., Pérez-Gussinyé, M., & Sobolev, S. V. (2014). Rift migration explains continental margin asymmetry and crustal hyper-extension. *Nature Communications*, *5*(1), 4014. https://doi.org/10.1038/ncomms5014

Buiter, S. J. H., & Torsvik, T. H. (2014). A review of Wilson cycle plate margins: A role for mantle plumes in continental break-up along sutures? *Gondwana Research*, *26*(2), 627–653. https://doi.org/10.1016/j.gr.2014.02.007

Christiansson, P., Faldeide, J. I., & Berge, A. M. (2000). Crustal structure in the northern North Sea: An integrated geophysical study. *Dynamics of the Norwegian Margin*, (McKenzie 1978), 15–40.

Corti, G., van Wijk, J., Cloetingh, S., & Morley, C. K. (2007). Tectonic inheritance and continental rift architecture: Numerical and analogue models of the East African Rift system. *Tectonics*, *26*, TC6006. https://doi.org/10.1029/2006TC002086

Dunbar, J. A., & Sawyer, D. S. (1988). Continental rifting at pre-existing lithospheric weaknesses. *Nature*, *333*(6172), 450–452. https://doi.org/10.1038/333450a0

Dunbar, J. A., & Sawyer, D. S. (1989). How preexisting weaknesses control the style of continental breakup. *Journal of Geophysical Research*, *94*, 7278. https://doi.org/10.1029/JB094iB06p07278

Erdős, Z., Huismans, R. S., van der Beek, P., & Thieulot, C. (2014). Extensional inheritance and surface processes as controlling factors of mountain belt structure. *Journal of Geophysical Research: Solid Earth*, *119*, 9042–9061. https://doi.org/10.1002/2014JB011408

Ferreira, T. S., Caixeta, J. M., & Lima, F. D. (2009). Basement control in Camamu and Almada rift basins. *Boletim de Geociências Da Petrobrás*, *17*(1), 69–88.

Fetter, M. (2009). The role of basement tectonic reactivation on the structural evolution of Campos Basin, offshore Brazil: Evidence from 3D seismic analysis and section restoration. *Marine and Petroleum Geology*, *26*(6), 873–886. https://doi.org/10.1016/j.marpetgeo.2008.06.005

Fichler, C., Odinsen, T., Rueslåtten, H., Olesen, O., Vindstad, J. E., & Wienecke, S. (2011). Crustal inhomogeneities in the Northern North Sea from potential field modeling: Inherited structure and serpentinites? *Tectonophysics*, *510*(1–2), 172–185. https://doi.org/10.1016/j.tecto.2011.06.026

Fossen, H. (1992). The role of extensional tectonics in the Caledonides of South Norway. *Journal of Structural Geology*, *14*, 1033–1046.

Fossen, H. (2010). Extensional tectonics in the North Atlantic Caledonides: A regional view. *Geological Society, London, Special Publications*, *335*(1), 767–793. https://doi.org/10.1144/SP335.31

Fossen, H., Gabrielsen, R. H., Faleide, J. I., & Hurich, C. A. (2014). Crustal stretching in the Scandinavian Caledonides as revealed by deep seismic data. *Geology*, *42*(9), 791–794. https://doi.org/10.1130/G35842.1

Fossen, H., Khani, H. F., Faleide, J. I., Ksienzyk, A. K., & Dunlap, W. J. (2016). Post-Caledonian extension in the West Norway-northern North Sea region: The role of structural inheritance. *Geological Society, London, Special Publications*, *439*(1), 465–486. https://doi.org/10.1144/SP439.6

Fullsack, P. (1995). An arbitrary Lagrangian-Eulerian formulation for creeping flows and its application in tectonic models. *Geophysical Journal International*, *120*(1), 1–23. https://doi.org/10.1111/j.1365-246X.1995.tb05908.x

Gleason, G. C., & Tullis, J. (1995). A flow law for dislocation creep of quartz aggregates determined with the molten salt cell. *Tectonophysics*, *247*(1-4), 1–23. https://doi.org/10.1016/0040-1951(95)00011-B

Guiraud, M., Buta-Neto, A., & Quesne, D. (2010). Segmentation and differential post-rift uplift at the Angola margin as recorded by the transform-rifted Benguela and oblique-to-orthogonal-rifted Kwanza basins. *Marine and Petroleum Geology*, *27*(5), 1040–1068. https://doi.org/10.1016/j.marpetgeo.2010.01.017

Harry, D. L., & Sawyer, D. S. (1992). A dynamic model of extension in the Baltimore Canyon Trough Region. *Tectonics*, *11*, 420–436. https://doi.org/10.1029/91TC03012

Hawkesworth, C. J., Cawood, P. A., Dhuime, B., & Kemp, T. I. S. (2017). Earth's continental lithosphere through time. *Annual Review of Earth and Planetary Sciences*, *45*(1), 169–198. https://doi.org/10.1146/annurev-earth-063016-020525

Hudec, M. R., & Jackson, M. P. A. (2004). Regional restoration across the Kwanza Basin, Angola: Salt tectonics triggered by repeated uplift of a metastable passive margin. *AAPG Bulletin*, *88*(7), 971–990. https://doi.org/10.1306/02050403061

Huismans, R., & Beaumont, C. (2011). Depth-dependent extension, two-stage breakup and cratonic underplating at rifted margins. *Nature*, *473*(7345), 74–78. https://doi.org/10.1038/nature09988

Huismans, R., & Beaumont, C. (2014). Rifted continental margins: The case for depth-dependent extension. *Earth and Planetary Science Letters*, *407*, 148–162. https://doi.org/10.1016/j.epsl.2014.09.032

Huismans, R. S., & Beaumont, C. (2003). Symmetric and asymmetric lithospheric extension: Relative effects of frictional-plastic and viscous strain softening. *Journal of Geophysical Research*, *108*(B10), 2496. https://doi.org/10.1029/2002JB002026

Karato, S., & Wu, P. (1993). Rheology of the upper mantle: A synthesis. *Science*, *260*(5109), 771–778. https://doi.org/10.1126/science.260.5109.771

Manatschal, G., Lavier, L., & Chenin, P. (2015). The role of inheritance in structuring hyperextended rift systems: Some considerations based on observations and numerical modeling. *Gondwana Research*, *27*(1), 140–164. https://doi.org/10.1016/j.gr.2014.08.006

Muñoz, J. A. (1992). Evolution of a continental collision belt: ECORS-Pyrenees crustal balanced cross-section. In *Thrust Tectonics* (pp. 235–246). Dordrecht, Netherlands: Springer. https://doi.org/10.1007/978-94-011-3066-0_21

Naliboff, J., & Buiter, S. J. H. (2015). Rift reactivation and migration during multiphase extension. *Earth and Planetary Science Letters*, *421*, 58–67. https://doi.org/10.1016/j.epsl.2015.03.050

Pedrosa-Soares, A. C., Noce, C. M., Wiedemann, C. M., & Pinto, C. P. (2001). The Araçuaí -West-Congo Orogen in Brazil: An overview of a confined orogen formed during Gondwanaland assembly. *Precambrian Research*, *110*(1-4), 307–323. https://doi.org/10.1016/S0301-9268(01)00174-7

Peslier, A. H., Woodland, A. B., Bell, D. R., & Lazarov, M. (2010). Olivine water contents in the continental lithosphere and the longevity of cratons. *Nature*, *467*(7311), 78–81. https://doi.org/10.1038/nature09317

Petersen, K. D., & Schiffer, C. (2016). Wilson cycle passive margins: Control of orogenic inheritance on continental breakup. *Gondwana Research*, *39*, 131–144. https://doi.org/10.1016/j.gr.2016.06.012

Pfiffner, O. a., & Ramsay, J. G. (1982). Constraints on geological strain rates: Arguments from finite strain states of naturally deformed rocks. *Journal of Geophysical Research*, *87*, 311–321. https://doi.org/10.1029/JB087iB01p00311

Piquè, A., & Laville, E. (1996). The Central Atlantic Rifting: Reactivation of Paleozoic structures? *Journal of Geodynamics*, *21*(3), 235–255. https://doi.org/10.1016/0264-3707(95)00022-4

Pysklywec, R. N., & Beaumont, C. (2004). Intraplate tectonics: Feedback between radioactive thermal weakening and crustal deformation driven by mantle lithosphere instabilities. *Earth and Planetary Science Letters*, *221*(1–4), 275–292. https://doi.org/10.1016/S0012-821X(04)00098-6

Schiffer, C., Stephenson, R. A., Petersen, K. D., Nielsen, S. B., Jacobsen, B. H., Balling, N., & Macdonald, D. I. M. (2015). A sub-crustal piercing point for North Atlantic reconstructions and tectonic implications. *Geology*, *43*(12), 1087–1090. https://doi.org/10.1130/G37245.1

Schmid, S. M., & Kissling, E. (2000). The arc of the western Alps in the light of geophysical data on deep crustal structure. *Tectonics*, *19*, 62–85. https://doi.org/10.1029/1999TC900057

Schmid, S. M., Pfiffner, O. A., Froitzheim, N., Schönborn, G., & Kissling, E. (1996). Geophysical-geological transect and tectonic evolution of the Swiss-Italian Alps. *Tectonics*, *15*, 1036–1064. https://doi.org/10.1029/96TC00433

Sleep, N. H. (2003). Survival of Archean cratonal lithosphere. *Journal of Geophysical Research*, *108*(B6), 2302. https://doi.org/10.1029/2001JB000169

Tack, L., Wingate, M. T. D., & Lie, J. (2001). Early Neoproterozoic magmatism (1,000–910 Ma) of the Zadinian and Mayumbian Groups (Bas-Congo): Onset of Rodinia rifting at the western edge of the Congo craton. *Precambrian Research*, *110*(1-4), 277–306. https://doi.org/10.1016/S0301-9268(01)00192-9

Thieulot, C. (2011). FANTOM: Two- and three-dimensional numerical modelling of creeping flows for the solution of geological problems. *Physics of the Earth and Planetary Interiors*, *188*(1–2), 47–68. https://doi.org/10.1016/j.pepi.2011.06.011

Thomas, W. A. (2006). Tectonic inheritance at a continental margin. *GSA Today*, *16*(2), 4–11. https://doi.org/10.1130/1052-5173(2006)016[4:TIAACM]2.0.CO;2

Tommasi, A., & Vauchez, A. (2001). Continental rifting parallel to ancient collisional belts: An effect of the mechanical anisotropy of the lithospheric mantle. *Earth and Planetary Science Letters*, *185*(1-2), 199–210. https://doi.org/10.1016/S0012-821X(00)00350-2

Tommasi, A., & Vauchez, A. (2015). Heterogeneity and anisotropy in the lithospheric mantle. *Tectonophysics*, *661*, 11–37. https://doi.org/10.1016/j.tecto.2015.07.026

Vauchez, A., Barruol, G., & Tommasi, A. (1997). Why do continents break-up parallel to ancient orogenic belts? *Terra Nova*, *9*(2), 62–66. https://doi.org/10.1111/j.1365-3121.1997.tb00003.x

von Nicolai, C., Scheck-Wenderoth, M., Warsitzka, M., Schødt, N., & Andersen, J. (2013). The deep structure of the South Atlantic Kwanza Basin —Insights from 3D structural and gravimetric modelling. *Tectonophysics*, *604*, 139–152. https://doi.org/10.1016/j.tecto.2013.06.016

Wiedemann, C. M., Medeiros, S. R., De Ludka, I. P., & Mendes, J. C. (2002). Architecture of Late Orogenic Plutons in the Araçuai-Ribeira Fold Belt, Southeast Brazil. *Gondwana Research*, *5*(2), 381–399. https://doi.org/10.1016/S1342-937X(05)70730-9

Willett, S. D. (1999). Rheological dependence of extension in wedge models of convergent orogens. *Tectonophysics*, *305*(4), 419–435. https://doi.org/10.1016/S0040-1951(99)00034-7

Wilson, J. T. (1966). Did the Atlantic close and then re-open? *Nature*, *211*(5050), 676–681. https://doi.org/10.1038/211676a0

Zalán, P. V., Severino, M., Rigoti, C. A., & Magnavita, L. (2011). An entirely new 3-D view of the crustal and mantle structure of a South Atlantica Passive Marg, Santos, Campos and Espírito Santo Basins, Brazil. In *AAPG Annual Conference and Exhibition* (pp. 1–3).